APOLLO: Meeting the Millimeter Goal

T. W. Murphy, Jr.[a], J. D. Strasburg[b], C. W. Stubbs[c], E. G. Adelberger[d], L. Tom[c], A. E. Orin[a], E. L. Michelsen[a], J. Battat[c], C. D. Hoyle[d], E. Swanson[d], E. Williams[a]

[a]UC San Diego, 9500 Gilman Dr.–0424, La Jolla, CA 92093-0424
[b]Pacific Northwest National Labs, P.O. Box 999, Richland, WA 99352
[c]Harvard University, 60 Garden St., Cambridge, MA 02138
[d]Box 351560, University of Washington, Seattle, WA 91895-1560

Abstract

As APOLLO (the Apache Point Lunar Laser-ranging Operation) progresses toward initial operation, we continue to explore ways in which our apparatus may introduce biases in our measurement. In this way, we can develop instrumentation and methodologies to remove or diminish these systematic bias sources. In this paper, we present a detailed study of the time behavior of our avalanche photodiode array devices. Most notably, we observed the dependence of avalanche report time as a function of spatial position of the illumination spot on the detector. If unchecked, the differing illumination pattern of the internal corner cube versus the lunar return would introduce a bias of roughly 100 ps (15 mm one-way). We discuss our implementation of an optical solution to the problem involving ground glass to match these illumination patterns. We also discuss the issue of thermal variations, and our strategy to minimize the impact of these on our differential timing scheme. The project status is summarized at the end.

1 Introduction

Since its undertaking, Lunar Laser Ranging (LLR) has performed the most precise tests of a number of gravitational phenomena, LLR has set the most stringent limits yet on the strong equivalence principle, the time-rate-of-change of Newton's gravitational constant, geodetic precession, gravitomagnetism, and departures from the $1/r^2$ gravitational force law [1, 2, 3, 4, 5]. As we continue to grapple with the inherent incompatibility between general relativity and quantum mechanics, precision tests of basic gravitational phenomenology become increasingly important. The fact that the universe appears to be accelerating in its expansion indicates that we may not yet fully understand large-scale gravity. Perhaps this is an indication of new physics such as the presence of a

Table 1: APOLLO Random Error Budget Per Photon

Random Error Source	Time Uncertainty (ps)	Range Error (mm)
Retroreflector Array Orientation	100–300	15–45
APD Illumination	60	9
APD Intrinsic	¡50	¡7
Laser Pulse Width	45	6.5
Timing Electronics	20	3
GPS-disciplined Clock	7	1
Total Random Uncertainty	136–314	20–47

scalar field modification to general relativity. Such scalar fields generically violate the equivalence principle, and also tend to introduce secular changes in the fundamental constants of nature [6].

2 Multi-photon Lunar Ranging

The Apache Point Observatory Lunar Laser-ranging Operation (APOLLO) [7] is a new effort in lunar ranging that aims to achieve one-millimeter range precision—representing an order-ofmagnitude improvement over other LLR efforts. Corresponding to about 7 ps of round-trip range delay, this puts stringent demands on the detection and timing of photons. The range determined from a single photon has much more uncertainty than one-millimeter, so that we must average many photon detections to arrive at the requisite precision. Table 1 lists the various sources of random uncertainty per photon. Our largest source of random error is the orientation of the retroreflector array, which changes as a function of lunar libration. The array can be tilted by as much as 10°, so that photons reflecting off of the nearest edge report a smaller range thatn photons that reflect off of the far edge. This effect can translate to roughly 950 ps of peak-to-peak range uncertainty for the largest reflector array. When the reflector array is oriented nearly perpendicular to the line of sight (about 15% of the time), we are most limited by the avalanche spreading phenomenon.

A full avalanche current is established once the entire active area of the detector element is participating in the avalanche. This state is attained most expediently if the avalanche begins in the center of the element and propagates outward from there. On the other extreme, if an avalanche begins at one edge, it could take roughly twice as long to establish full current. The rest of the random error budget includes things such as the effects of the finite laser pulse width, other temporal uncertainties in the APD detectors, timing electronics jitter, and timebase jitter.

All together, one-millimeter range precision demands that we acquire enough data points such that $\sigma_{\rm final} = 1\,{\rm mm} = \sigma_{\rm photon}/\sqrt{N}$, where N is the number of photons collected, each with intrinsic uncertainty $\sigma_{\rm photon}$. In the case of $\sigma_{\rm photon} = 50$ mm, one needs 2500 photons to achieve the requisite reduction in random uncertainty. By comparison, the currently operating LLR stations

build normal points out of typically 10–100 photons. Realistic attempts to quantify the range signal from the 3.5 m telescope at the Apache Point Observatory (in southern New Mexico at an altitude of 2800 m) result in predictions of several photons per pulse. Taking one photon per pulse as a baseline, at 20 Hz pulse repetition rate we would expect to net 1200 photons per minute, so that our millimeter goal may be realized on a timescale of a few minutes. Previous publications document the photon signal expectations in greater detail [8, 9].

Two aspects of this multi-photon-per-pulse regime deserve special mention. The first is that the detector only responds to the first photon to trigger an avalanche. In order to avoid biasing the range measurement to shorter values, multiple detector elements must be available to collect photons. Because of this, we are using an array detector [10], discussed below. The second point is that even at a photon rate 100 times lower than calculated expectations, we will detect roughly one photon per second. This rate is high enough to allow real-time system optimization in regard to telescope pointing, transmitter/receiver pointing offset (for velocity aberration), beam divergence and telescope focus. The two dimensional detector array facilitates the pointing corrections. The net result is that it should be possible to "steer" onto a return rate close to expectations, even starting at a rate two orders-of-magnitude lower.

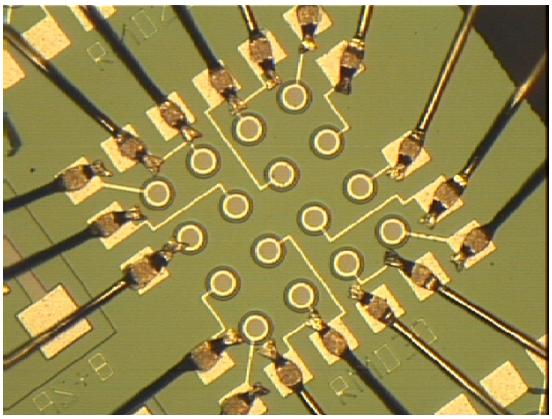

Figure 1: Lincoln Labs APD array: 30 μm active areas on 100 μm centers. The array provides multiple detectors to accommodate a multi-photon return, and also allows closed-loop signal tracking.

The APOLLO detector is a 4×4 array of avalanche photodiode (APD) elements: each is 30 μm in diameter, separated by 100 μm (Figure 1—this spacing limits crosstalk). Thus 16 "buckets" are placed in the receiver stream, and sized such that the "pixels" oversample the seeing-limited spot size from the lunar array. The spacing between elements results in a low fill-factor, so that we use a micro-lens array in front of the detector to recover nearly 100% fill-factor. The lenslet array is itself located at a re-imaged telescope focus. In this way, each lens, or "pixel" represents a spatial position on the sky—in our case about 0.35 arcseconds on a side. The detector array is then

located roughly one focal-length away from the lenslets, so that a pupil image is formed within the confines of the 30 μm detector element (Figure 2). By tracking the average hit rate for each APD element, an illumination pattern is built up, and we can tell if the lunar return is centered on the array. The formation of a pupil image on the APD element means that in effect an image of the primary mirror is formed there. Returned lunar photons strike the telescope entrance aperture (primary mirror) in random locations, so that the APD element is roughly uniformly illuminated (except for the central obstruction from the secondary mirror).

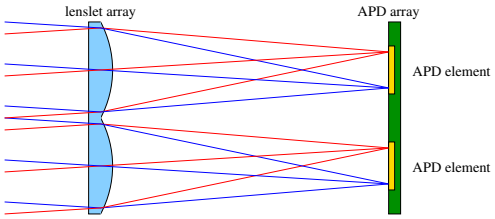

Figure 2: The microlens—or lenslet array—concentrates incoming light onto the individual APD elements. The lenslet itself is located at a telescope focus. The rays in the figure are color-coded to indicate origin of location on the primary mirror. An image of the primary is formed on each APD element.

The spread in location of the incident photon within the APD element translates to a timing uncertainty, discussed in Section 3. One dangerous aspect of this spread regards the fiducial corner cube. A corner cube is located in the exit aperture of the telscope to catch light leaving the primary mirror en-route to the moon. Photons returned from this corner cube are detected in a way that is identical to the lunar retroreflector returns—identical in terms of optical path, signal level, detection, and timing. The corner cube thus provides a time fiducial for the outgoing pulse. The danger is that the corner cube does *not* spread photons uniformly across the telescope aperture (and thus the detector element), but rather in a well-confined spot. This has the effect of biasing the differential measurement since the average time-to-avalanche may differ between lunar and fiducial photons. It is for this reason that we have studied this problem in detail.

3 Avalanche Initiation Location

When a photon impinges on an avalanche photodiode, it penetrates some distance before creating an electron-hole pair in the semiconductor. For silicon, the characteristic penetration depth at a wavelength of 532 nm is about 1.0 μm. The penetration depth varies from photon to photon, leading to a spread in the initial depth of the electron-hole pair. An electric field drives the electron toward the p-n junction and multiplication region. At a saturation velocity of about 10^5 m/s, (0.1 μm/ps), the variable penetration depth translates to roughly 10 ps of variability in when an

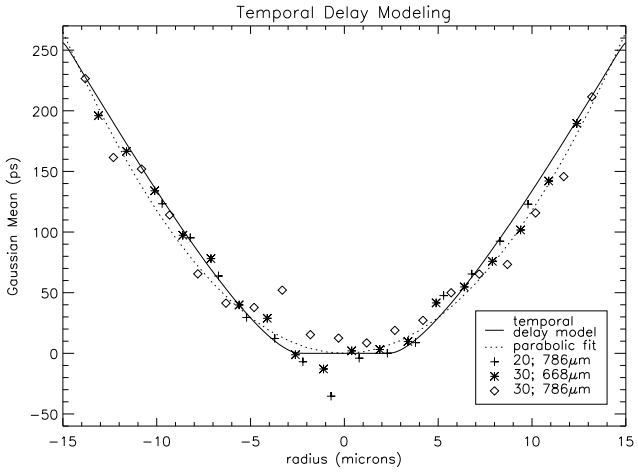

Figure 3: Spatial scans of avalanche initiation delay for two different devices at two different wavelengths. A crude parabolic fit is plotted, as well as a model based on linear spread of the avalanvhe front.

electron reaches the multiplication region. At this point, a microplasma of avalanching electron-hole pairs spreads across the disk-shaped multiplication region. It may be assumed that the front of this plasma propagates across the silicon at a uniform speed—presumably not much slower than the thermal speed of an electron in silicon (1.2×10^5 m/s). In this model, an avalanche initiated in the center of the detector element reaches saturation current (the whole disk in avalanche) sooner than an avalanche initiated at the edge of the element. Variation my be expected to be > 150 ps for a 30 μm element.

We have observed this effect in our APD elements, by illuminating the detector with a pulsed laser spot a few microns across, and measuring report time while scanning this spot across the spatial extent of the array. For this study, we used a short-pulse laser diode with a pulsewidth of 40 ps and a wavelength of 786 nm. The shift in avalanche report time is tracked as a function of spatial position, producing data like that presented in Figure 3. Both the 20 μm and 30 μm devices follow the same rules, showing a delay that evolves quadratically as a function of position away from the center. Models that allow the microplasma front to grow linearly until it hits an edge of the element, and an avalanche trigger at some fraction of the saturation current (current is assumed to be proportional to area) produce results consistent with the data in Figure 3, whose simplified form is approximately $1.2r^2$ ps, where r is the distance from the element center, in microns. We can fit this model to the data with a single parameter, corresponding to the speed of the microplasma front. In doing so, we infer a speed of 3.5×10^4 m/s, or roughly 1/3 the electron thermal velocity.

This microplasma development phenomenon means that any specific illumination pattern on the APD element will have an associated delay, but also a spread in the report times. Any small

spot or thin, centered annulus will have little spread, but the intended illumination for APOLLO (most of the active area) will result in a spread of about 65 ps, and a delay of 115 ps compared to a centrally-initiated avalanche.

Though the random uncertainty arising from the illumination pattern is unwelcome, a more serious problem exists in the potential bias introduced in our "differential" measurement scheme. The placement of a corner cube in the exit aperture of the telescope allows a near real-time comparison to the lunar return sharing the same optical path, detectors, and timing system. Only the signal level is different, and this is adjusted to roughly match the lunar signal via a battery of attenuators on rotating glass disks. The statement that the two returns follow the same optical path is, however, not strictly true. The fiducial photons only strike a small part of the primary mirror. Because this mirror is imaged onto the APD array elements, the fiducial photons then hit each detector in one small spot. Therefore, the avalanche initiation delay from the fiducial corner cube will not in general match the average delay experienced by the lunar photons. If left uncorrected, this would amount to a range bias of the order of 100 ps, or about 15 mm.

4 Eliminating the Avalanche Initiation Bias

The range bias resulting from the different illumination of lunar and fiducial photons on the detector is not in itself a cause for concern if it is static. This bias would be systematic in the data analysis, and could be fit out. However, it is difficult to guarantee that the corner cube return always hits the same spot on the detector, as even slight optical tweaks could affect this. For instance, if the corner cube is located near the edge of the primary mirror, the fiducial photons would strike the outer edge of the APD element, where the slope in the delay curve is large (r^2 dependence: Figure 3). For our system, a motion of one micron near the edge of the detector would result in a delay difference of about 40 ps. A variable range delay of even one sixth of this would negatively impact our goal of long-term millimeter range precision. We require a solution to this problem that is robust against changes in optical alignment.

By intermittently placing a ground glass diffuser into the optical beam at the time of laser fire, we can effectively spread the fiducial photons from the corner cube into a distribution that mimics the lunar return. This works properly only in certain locations within the optical beam. The diffuser randomizes angle (15° FWHM Gaussian is typical), and this has the effect of mimicking the lunar photons only at a focal plane (Figure 4). The resulting nearly-uniform illumination at the detector reduces our bias between lunar and fiducial events to 3 ps, which can easily be estimated and removed at the sub-picosecond level.

Because the diffuser is located at a focus, the illumination pattern at the diffuser is small—and this is an advantage, because the diffuser must be switched in and out at the repetition rate of the laser. The switching requirement isn't essential, but one otherwise looses flux in the lunar return by the action of diffusion (much of the light no longer finds the detector). The APOLLO optical system employs a spatial filter for background reduction, with an aperture of 3 arcseconds

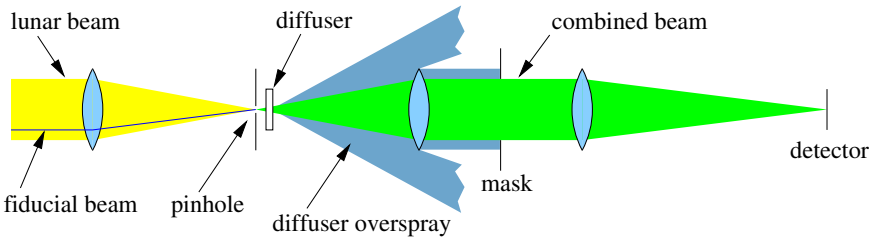

Figure 4: Schematic of diffuser location within the receiver. Within the collimated input beam, the fiducial occupies a very small part of the cross-section—corresponding to the area the corner cube covers on the primary mirror. After the diffuser and mask, the lunar and fiducial photons have identical optical paths.

(400 μm). This is an ideal location for the diffuser, which we have implemented as a rotating disk with one quadrant ground into a diffuser. A mask located downstream of the spatial filter in a section of collimated beam ensures that the lunar and fiducial illumination patterns are identical on the detector even in the presence of optical misalignment. The detector and mask form conjugate image planes.

We have chosen to use a single-quadrant diffuser rotating at half the laser repetition rate rather than a half-covered disk rotating at full speed. This results in every *other* fiducial return passing through the diffuser. The fiducial returns then alternate between biased-but-sharp and unbiased-but-blurry. In this way, it is possible to recover the full time-precision associated with the laser pulse width, the APD intrinsic jitter, and the timing electronics jitter without intentionally introducing the rather large timing spread associated with the avalanche initiation variability. Thus this non-diffused fiducial serves as a diagnostic of the temporal quality of our laser pulse, detector, electronics, etc. At the same time, every other shot is spread out across the APD element in such a way as to mimic the delay associated with the spread-out lunar photons. By comparing the two, we can directly monitor the bias, and apply this bias correction to the sharp pulse, thus preserving the best that both have to offer. Ultimately, we will use only the sharp (un-diffused), but bias-corrected fiducial returns. Because the avalanche initiation spread dominates the error budget, using only half of the fiducial photons in this way is more than compensated by the sharpness of the un-diffused pulse.

4.1 Physical Implementation

The quadrant opposite the diffuser has a coating for attenuation (approximately 1 O.D.) to balance the signal loss associated with the light diffusely scattered outside of the detector's active area. In this way, differential biases associated with signal level (e.g., first-photon bias) is avoided. Our quadrant diffuser disk is mounted on a rotating shaft along with two other quadrant attenuators—each clear in the two lunar quadrants and attenuating in the two fiducial quadrants. One of the two

attenuator disks is a fixed value, while the other disk is an angularly variable attenuator spanning 1.5 optical densities. By tuning the phase of the quadrant diffuser/attenuator assembly, one may adjust the overall attenuation of the fiducial path. Given 16 available detectors, a 10% hit rate corresponds to roughly two fiducial photons per shot. At this level, the first-photon bias is small, and may be reasonably corrected. Most of the attenuation along the fiducial path is generated at the transmit/receive switch, where the dielectric coatings on the front and back of the rotating disk result in about 10^{-6} transmission. The quadrant diffuser/attenuator assembly contributes another ~ 4 orders-of-magnitude of fiducial attenuation.

5 Thermal Effects

The differential measurement scheme employed by APOLLO in essence measures the distance between a fiducial corner cube located near the telescope secondary mirror and the corner cube array on the moon. The same exact optical path (with the exception of a few optical coatings) is used for both, as well as the same detection/timing scheme. By making the two measurements as identical as possible, we are largely insensitive to intermediate- or long-term drifts. As long as the system is stable over the ~ 2.5 sec of round-trip travel, the differential approach is valid.

One of the most worrisome potential failures of the differential measurement scheme is the time-to-digital converter that APOLLO uses for its high-resolution time measurement. The TDC measures the time between an ECL pulse generated from a detected photon (the START) and a second ECL pulse (STOP) generated based on the 50 MHz time reference. The Phillips Scientific model 7186 TDC measures a 100 ns range to 25 ps resolution, with a typical RMS uncertainty of 13 ps. The reported bin number (12-bit digital time) for a given Δt is a roughly linear function, $N_{\rm TDC} = a + b\Delta t$, with "offset," a, and "gain," b. Both the offset and gain are known to vary with temperature. From Figure 5, it is seen that the TDC "gain" varies by approximately 160 parts per million per degree Celsius. This becomes important if the phasing of the lunar and fiducial signals with respect to the 50 MHz clock are different, so that the Δt values are mismatched. If these time offsets from the 50 MHz reference could be made to be the same, there would be no need to understand the parameters a and b, as these would perfectly cancel in the differential measurement. If the Δt values differ by T nanoseconds, then the temperature-induced variations will amount to $\Delta b/b \times T$. If T is allowed to be half of the TDC's range, or 50 ns, then a 5 ps bias requirement restricts gain variations to $\Delta b/b < 10^{-4}$, implying a thermal stability (or knowledge) of about 0.5°C.

We can significantly reduce this burden by arranging to use the same range of the TDC for both lunar and fiducial measurements. On a shot-by-shot basis, it is impossible to control where either the lunar or fiducial photons land with respect to the 50 MHz frequency standard, since the laser fire time and the lunar distance are asynchronous with this clock. But we *can* control *which* clock pulse is used as the STOP for any event. Thus each photon signal can be maintained within a 20 ns range. Moreover, the two ranges can be made to exactly overlap, so that the TDC measurements

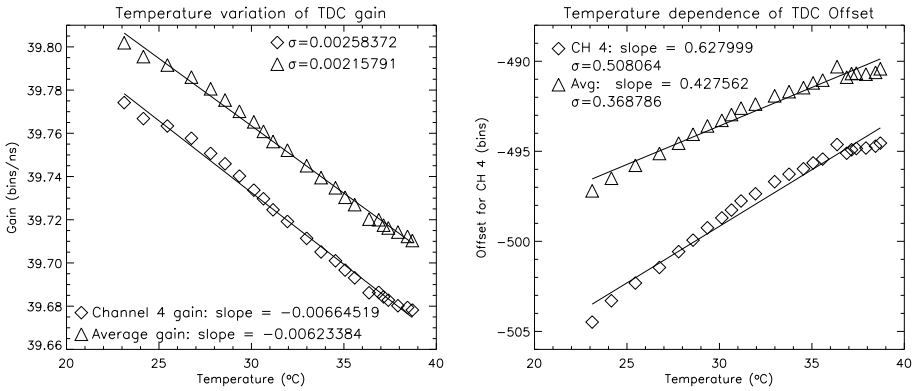

Figure 5: TDC gain and offset as a function of temperature. Plots are shown for an individual channel, as well as for the average of all 16. The slope of 0.0064 bins/ns per C° translates to 160 ppm per C°.

are on average the same for both signals. If we control the average TDC position of the two signals relative to each other to 1 ns, our 5 ps bias requirement now implies an acceptable temperature range of 25°C. Maintaining the relative position of the two signals to 1 ns is not very challenging, given that we will accumulate enough data to determine the relative positions within a few seconds, and the lunar range estimate varies by far less than this (typically ¡ 100 ps) over the anticipated hour timescale of lunar ranging operation.

Though the forced overlap in TDC-space reduces the systematic thermal influence, we will supplement our knowledge with temperature measurements at several key locations within the TDC unit. We will also conduct a TDC calibration every few minutes wherein a series of START/STOP pairs separated by integral multiples of 20.00ns (derived from frequency standard) are sent to the TDC to determine the gain, offset, and low-order nonlinearity of each of the 16 TDC channels. This process takes only five seconds at 1000 START/STOP pairs per pair separation. Thus we can perform this routine frequently.

6 Project Status

APOLLO expects to be operational before the close of 2005. At present (Jan 2005), the laser is mounted on the telescope and housed in an insulating enclosure. Two other insulated enclosures have also been constructed to house the electronics, power supplies, computer, and chillers. Much effort has gone into thermal considerations—not only for temperature control/stability, but also to limit the heat flux into the dome to less than 50 W at all times. Most of the optical train for the receiver is built and tested. The APD array has been thoroughly tested and the final set of electronics is in fabrication. The central detection-timing system is well-established, and turning out

~ 20 ps performance. Among the major tasks that remain before initial operation are: establishing the umbilicals cabling/tubing from the static structures to the laser enclosure on the moving telescope; fabricating the remaining optical mounts; installing a micro-lens array onto the APD array; and developing the user interface software. We anticipate initial lasing in July 2005, and science operation in the following fall.

References

[1] Williams, J. G., Turyshev, S. G., & Boggs, D. H., "Progress in Lunar Laser Ranging Tests of Gravity," *Phys. Rev. Lett.*, **93**, 261101, (2004)

[2] Williams, J. G., Boggs, D. H., Dickey, J. O., & Folkner, W. M., "Lunar Tests of the Gravitational Physics," *Proceedings of the Ninth Marcel Grossman Meeting*, Rome, Italy, June 2000, World Scientific Publications, R. Jantzen, ed., (2001)

[3] Nordtvedt, K., "Lunar Laser Ranging—A Comprehensive Probe of Post-Newtonian Gravity," arXiv:gr-qc/0301024

[4] Anderson, J. D., & Williams, J. G., "Long-Range Tests of the Equivalence Principle," *Class. Quantum Grav.*, **18**, 2447, (2001)

[5] Williams, J. G., Newhall, X. X., & Dickey, J. O., "Relativity parameters determined from lunar laser ranging," *Physical Review D*, **53**, 6730, (1996)

[6] Damour, T., & Nordtvedt, K., "Tensor-scalar cosmological models and their relaxation toward general relativity," *Phys. Rev. D*, **48**, 3436, (1993)

[7] Murphy, T. W., Strasburg, J. D., Stubbs, C. W., Adelberger, E. G., Angle, J., Nordtvedt, K., Williams, J. G., Dickey, J. O., & Gillespie, B., "The Apache Point Observatory Lunar Laser-ranging Operation (APOLLO)," *Proceedings of the 12$^{\rm th}$ International Workshop on Laser Ranging*, (2000)

[8] Murphy, T. W., Adelberger, E. G., Strasburg, J. D., & Stubbs, C. W., "APOLLO: Multiplexed Lunar Laser Ranging," *Proceedings of the 13$^{\rm th}$ International Workshop on Laser Ranging*, (2002)

[9] Murphy, T. W., Adelberger, E. G., Strasburg, J. D., Stubbs, C. W., & Nordtvedt, K., "Testing gravity via next-generation lunar laser-ranging," *Nuclear Physics B*, **134**, 155, (2004)

[10] Strasburg, J. D., Murphy, T. W., Stubbs, C. W., Adelberger, E. G., Miller, D. W., & Angle, J., "Lunar Laser Ranging Using Avalanche Photodiode (APD) Arrays," *Proceedings of the SPIE: Astronomical Instrumentation*, **4836**, 387, (2002)